The impact of hot roll temperature on the microstructure and corrosion resistance of super duplex stainless steel, which is used to coat mild steel in seawater environments

Lusiana [a], M.S. Anwar [a], P.A. Paristiawan [a], A.N. Syahid [a], R.N. Hakim [a], Y. Lestari [a], M. Perkasa [b], K. Prijono [c]

[a] Research Center for Metallurgy, National Research and Innovation Agency (BRIN), South Tangerang, Jakarta, Indonesia
[b] Laboratory of Structural Strength, National Research and Innovation Agency (BRIN), South Tangerang, Jakarta, Indonesia
[c] Advanced Chemical and Advanced Physics Imaging Laboratory, National Research and Innovation Agency (BRIN), South Tangerang, Jakarta, Indonesia

*Corresponding author: lusianand@yahoo.com, lusi001@brin.go.id
Author: msyifulan04@gmail.com, permana.andi@gmail.com, adiole75@yahoo.com, rahmanisa.hakim@gmail.com, yuli035@brin.go.id, mustasyar.perkasa@brin.go.id, Kusd001@brin.go.id

(Received 26 September 2024; Accepted 27 December 2024)

Abstract

A new material that can be used to replace single steel in high-strength tanks is mild steel cladding Super Duplex Stainless Steel (SDSS). The method of making multilayer Super Duplex Stainless Steel (SDSS) is mild steel cladding, many processes are carried out such as welding *methods plasma Direct Energy Deposition (DED), laser, and electro-slag strip. In the manufacturing industry, hot rolling is a simple process. Because the procedure is quick and uses inexpensive, traditional equipment, it is referred to as a simple method. The use of seawater was made because salt conditions are conducive to corrosion. The impact of temperatures of 900°C, 1000°C, and 1050°C on the microstructure and corrosion resistance of hot rolling materials is investigated in this work. Investigating corrosion resistance through test microstructure and material properties using metallography, X-ray diffraction, Electrochemical Impedance Spectroscopy (EIS), and Scanning Electron Microscope (SEM) is the main goal of this work. The study's findings demonstrated that when hot rolling temperature increased, carburization and decarburization took place and corrosion resistance declined.*

Keyword: SDSS, Mild Steel, Hot Rolling, carburization, decarburization

1. Introduction

In industrial settings, carbon steel is often prone to corrosion, and a high level of corrosion resistance is necessary for both economical and secure operation. Crude oil is utilized in the oil and gas sector because it contains specific chemical constituents that might speed up corrosion, like sulfur, nitrogen, and aromatic resins. Using organic or inorganic inhibitors that shield the steel surface by creating a passive protective layer is the most common method of increasing corrosion resistance [1], [2]

A unique iron alloy known as duplex stainless steel comprises balanced phases of austenite (γ) and ferrite (δ) in its microstructure. In situations containing acids, acid chlorides, seawater, and chemicals, this two-phase structure produces steel with excellent strength, toughness, and

corrosion resistance [2], [3], [4]. The use of super duplex stainless steel has increased in areas that are extremely corrosive, such as the production of paper and pulp, heat exchangers, chemical storage tanks, and oil and gas infrastructure. For the uses listed above, duplex stainless steel alloys that are resistant to corrosion are more corrosion-resistant than low-carbon steels, albeit they come at a significantly higher material cost [5].

In previous studies in the manufacture of multilayer stainless steel and carbon steel using several methods, namely welding methods [3],[6],[7][8] plasma Direct Energy Deposition (DED)[9], laser[10], [11], [12], [13], and electro-slag strip[14]. The hot and cold rolling techniques that are used on super duplex steel do not significantly affect the material's surface. Nevertheless, cold rolling is preferable than hot rolling for corrosion resistance [15]. Low-carbon steel is hot rolled to obtain better mechanical properties, where the mechanical properties are increased compared to cold working [16].

Although the surface of super duplex steel is not significantly damaged during the hot or cold rolling processes, the cold rolling method improves corrosion resistance over the hot rolling process. [17]. To obtain better mechanical properties, mild steel is hot rolled which improves the mechanical properties compared to cold working [18].

Increasing mechanical qualities and corrosion resistance is the goal of creating multilayers between two different materials [19]. When compared to cold working, the corrosion resistance of multilayer duplex made of carbon steel that has been hot rolled and aged produces precipitates [20]. Meanwhile, corrosion can be produced effectively using the electro slag strip method with different solutions [21]

The aim of this study is to investigate the corrosion resistance of mild steel Super Duplex Stainless Steel (SDSS) - layer multilayer systems during the hot rolling process in salt environments. The focus of this study is to investigate corrosion resistance by using test microstructure and material properties Scanning Electron Microscope (SEM), metalografi, X-Ray Diffraction dan Electrochemical Impedance Spectrcopy (EIS).

2. Materials and Methods

Super duplex and low carbon steel materials were cut to the same size, and to prevent the two materials from shifting after rolling, the ends of the materials were welded together. Then, employing temperatures of 900°C, 1000°C, and 1050°C, the hot rolling process was completed. This research experiment can be seen in the schematic diagram in Figure 1.

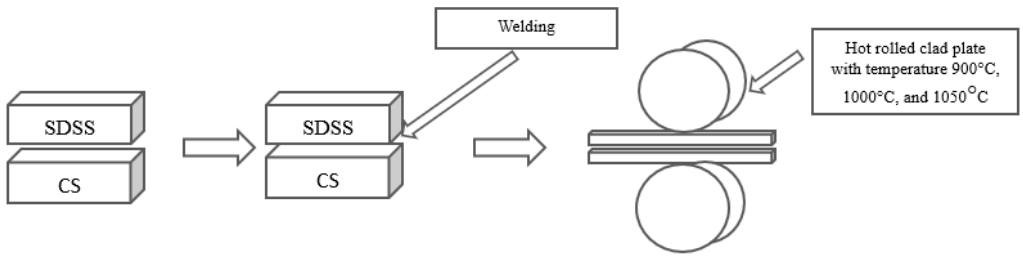

Figure 1. Schematic diagram for hot rolling

Table 1 shows the factors used in this investigation. To facilitate testing, the material was chopped after the temperature was changed, and then it was mounted using resin. Sandpaper roughness size for grinding of 120, 240, 400, 600, 800, 1000, and 1200, 1500, 2000 was used to grind the samples. The JEOL JSM IT-200 LA was then used to conduct the test using a scanning electron microscope (SEM). Meanwhile, Panalytical Empiren is being used for XRD. After polishing the sample with cloth disks containing diamond paste that had a size of 0.3µ, Kalling's solution was used to etch the sample in order to view its microstructure. An Olympus microscope, which is used for metallography, was one of the tools.. With a test electrolyte of 5% NaCl aqueous solution, all electrochemical experiments were conducted in a three-electrode electrochemical cell. Coated specimens serve as the working electrode, while graphite plates and saturated calomel electrodes (SCE) serve as the counter and reference electrodes. Potentiostat/galvanostat/ZRA Gamry 3000 and other test instruments were used.

Table 1. Research variables

Sample/code sample	Temperature Rolling (°C)
Mild steel (1)	-
SDSS (2)	-
Cladding (3)	900
Cladding (4)	1000
Cladding (5)	1050

Table 2. Chemical composition of mild steel and SDSS (wt%)

Material	**C**	**Si**	**Mn**	**Cr**	**Mo**	**Ni**	**P**	**S**	**Fe**
Mild steel	0.14	0.16	0.69	0.11	0.024	0.097	<0.01	<0.01	bal
SDSS	0.01	0.37	0.34	24.92	3.87	6.36	<0.01	<0.005	bal

Table 2 illustrates that carbon steel materials are covered by ASTM SA 210A1 or ASTM 213 standards that are frequently applied to pipes, such as those made of austenitic and ferritic steel for superheaters, heat-exchanger tubes, and boilers [22]. As a super duplex stainless steel (SDSS) material, it is mostly utilized in the oil and gas industry, particularly for offshore platforms, heat exchangers, structural elements, and architectural elements. Type UNS: S32750 is a variant of stainless steel alloy [23]

3. Result and Discussion

3.1. Microstructures

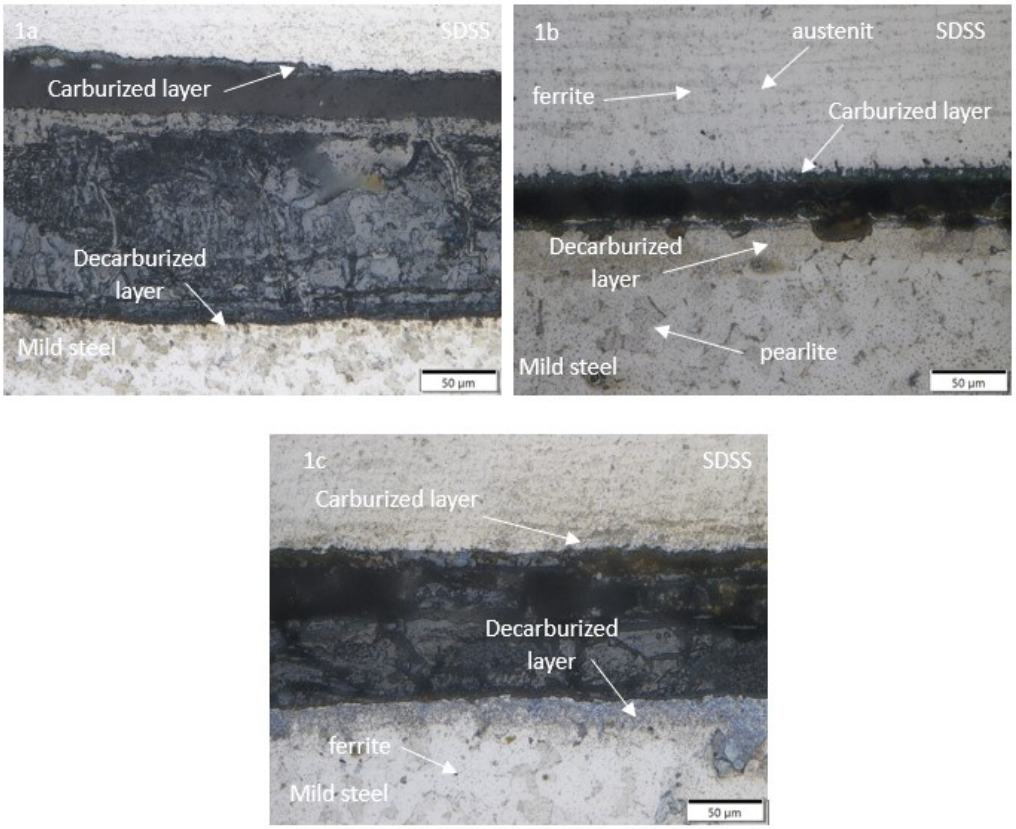

***Figure 2**: Results of Metallographic Test . The temperatures at which hot rolling occurs are (1a) 900°C, (1b) 1000°C, and (1c) 1050°C*

The outcomes of metallographic testing with Kalling's etching are shown in Figure 2. Mild steel, the decarburization area, the SDSS, and the carburization area are the four components of the microstructure study of samples with variations in hot rolling temperatures of 900°C, 1000°C, and 1050°C. High temperatures cause metallurgical bonding, or the reciprocal diffusion of elements [24]. Figure 2(a) shows that the decarburization layer that forms on the mild steel side is not particularly apparent, and the carburization layer on the SDSS side is not very thick. The carburization and decarburization layers are thicker in Figure 2(b) from both the mild steel and SDSS sides than in Figure 2(a), while the carburization layer is thinner in Figure 2(c) than in Figure 2(b). The cladding contact exhibits a uniform and clearly visible decarburization layer on the mild steel side [25]. Diffusion of components during heating results in carburization zones and decarburization [26]. The initial driving force for the diffusion of elements is provided by the considerable differences in the amount of C, Cr, Fe, and other elements between mild steel and SDSS. Ferrite and pearlite make up the structure of the mild steel region. The carbon atoms from the mild steel close to the interface diffuse across the layer boundary to the SDSS side during the heating process in the decarburization zone, which lowers the carbon content in pearlite and causes it to change to a ferrite structure upon raising the rolling temperature. There is just a coarse ferrite structure in the decarbonization zone as a result. C atoms are added to the SDSS side in the carburization zone, whilst Cr atoms from the SDSS diffuse into the mild steel in the vicinity of the interface. In the cladding layer, SDSS starts to change into a thick austenite structure due to a rise in the element C, which promotes austenite, and a decrease in the element Cr, which promotes ferrite. Element diffusion has little effect on the ferrite + austenite structure

located far from the cladding. When the heating temperature rises, the grain size, decarburization zone, and carburization zone all get wider [27]

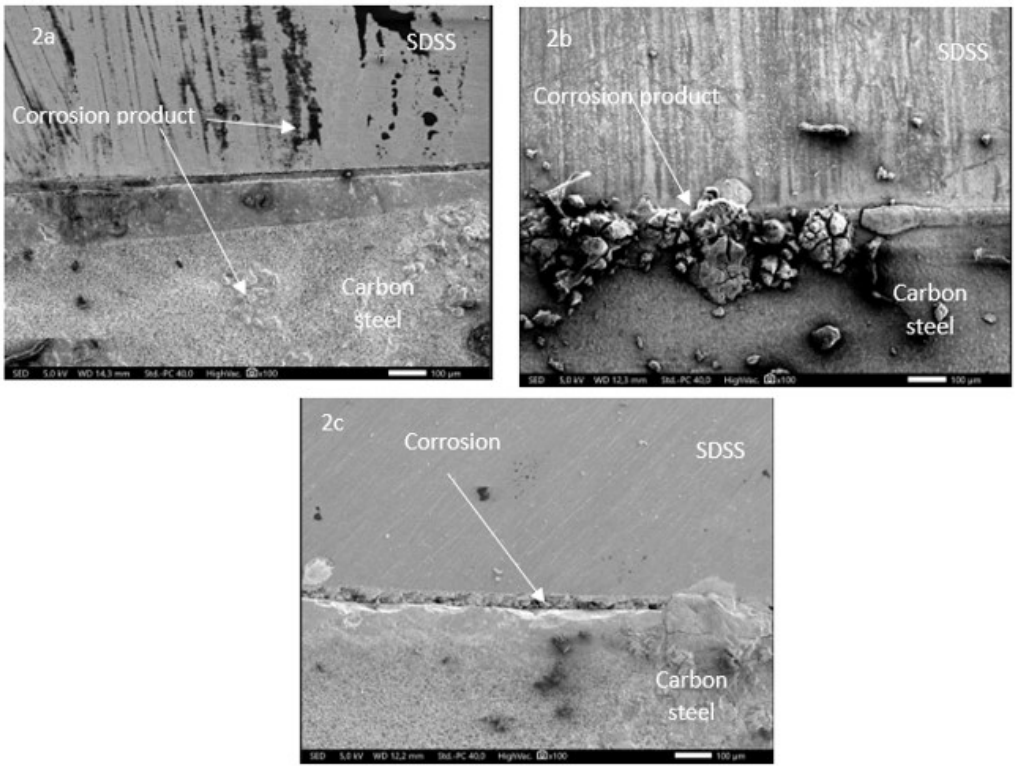

Figure 3. *SEM results after the hot rolling process, 2(a) rolling temperature 900℃, 2(b) rolling temperature 1000℃, 2(c) rolling temperature 1050℃ .*

Figure 3(a) illustrates how the surface of SDSS is corroded, as indicated by the black color present; on the surface of low-carbon steel, the corrosion product takes the form of powder. While corrosion does occur on the cladding, it is not as bad as it is on the surface. Figure 3b shows that corrosion on the cladding results on the low carbon steel side, but as compared to the low carbon steel side, the corrosion on the SDSS surface is not as severe.

Figure 3c shows corrosion on the low-carbon steel surface and cladding. The corrosion appears porous and eats away at some of the cladding that results. The corrosion that develops on the low carbon steel surface further from the cladding is nearly identical to that shown in Figure 3a. As explained in the microstructure results, this damage is caused by the decarburization process in the cladding results, resulting in corrosion products and damaged cladding results.

3.2. XRD result

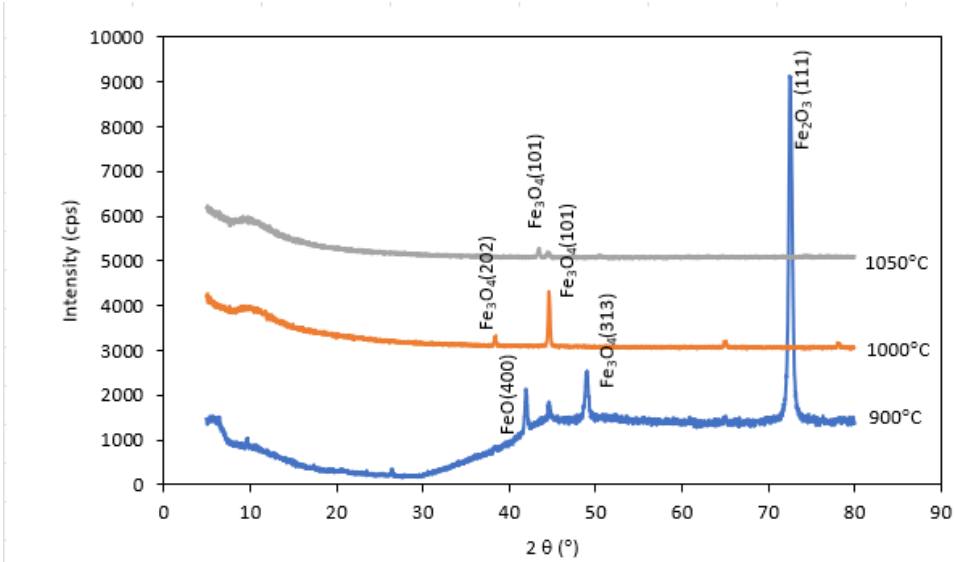

***Figure 4**. XRD Pattern of SDSS mild steel cladding with hot rolling temperature 900℃, 1000℃, dan 1050℃.*

The XRD graph in Figure 4, created with Macth! Software, shows that the cubic crystal form with lattice parameter (a) 3.6710 Å has Fe peaks (111), (313), and (400) at a hot rolling temperature of 900°C. The peaks that develop at 1000°C hot rolling temperature are (101) and (202), with a cubic lattice parameter (a) of 2.8714 Å; at 1050°C hot rolling temperature, the peak that forms is (101), with a lattice parameter (a) of 3.5140 Å. The size of the lattice parameter varies at different hot rolling temperatures, as can be observed here.

Iron A has two crystal structures: FCC (Face Body Center) and BCC (Body Cubic Center). In contrast to the FCC structure, iron atoms in the BCC crystal structure have more mobility to travel and diffuse. This is because the atomic arrangement in the BCC structure is less dense and more open, with greater interstitial gaps between the atoms. This facilitates the easier diffusion and mobility of iron atoms inside the crystal lattice. In comparison, the iron atom arrangement in the FCC crystal structure is denser and has smaller interstitial spaces. In comparison to BCC iron, this restricted atomic mobility makes it harder for iron atoms to diffuse through the lattice, leading to a reduced self-diffusion coefficient [28].

From the Match! Database A hot rolling temperature of 900 was used to generate the space group Fm-3m (225). At 910°C, iron exhibits a Face Cubic Center (FCC) structure [28], [29] The resulting space group is lm-3m with a Body Cubic Center (BCC) structure at 1000°C

The crystal structure returns to the Face Cubic Center (FCC) around 1050°C [29]. This variation results from anisotropic iron's ability to form distinct crystal structures at various temperatures before returning to its original form.

3.3. Electrochemical properties

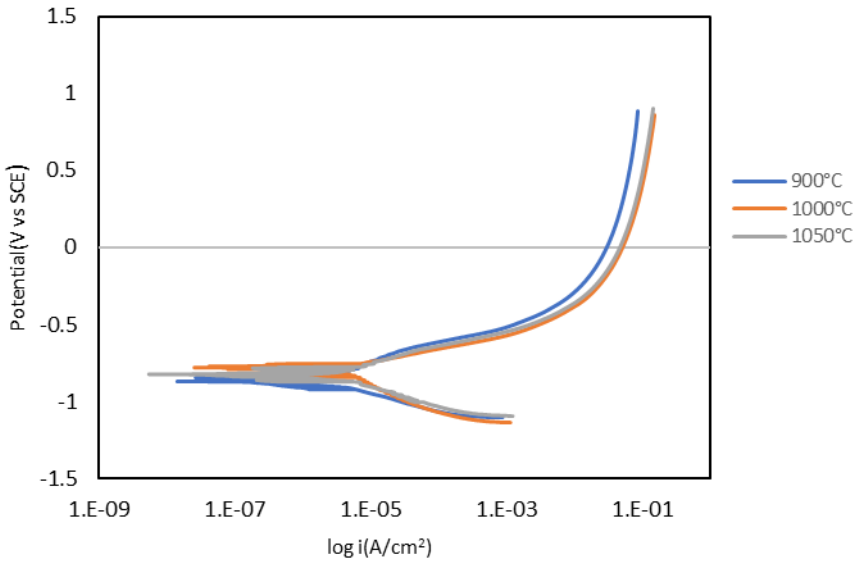

***Figure 5**. The potentiodynamic polarization curve of super duplex mild steel cladding by variation of hot rolling temperature in 5% NaCl solution*

The multilayer multilayer test curve for carbon steel and SDSS at room temperature using a 5% NaCl solution is shown in Figure 5. In this instance, the NaCl solution was chosen since it is a solution that is utilized for multilayer corrosion testing in seawater on SDSS and mild steel [30], [31].

Table 3. Electrochemical parameters of potentiodynamic test results

sample	E_{corr} (mV)	I_{corr} (A/cm^2)	Corrosion rate (mmpy)
1	-647.1	7.216 x 10^{-6}	88.77 x 10^{-3}
2	-615.7	3.571 x 10^{-6}	41,46 x 10^{-3}
3	-1.023	68.10 x 10^{-6}	790.5 x 10^{-3}

The corrosion mechanism in superduplex mild steel cladding is illustrated in Figure 5 by the potential-dynamic curve of polarization of the cladding caused by changes in hot rolling temperature in a 5% NaCl solution. In comparison to the change in hot rolling temperature, the resulting curve is not that different.

The capacity of a metal to react electrochemically with its surroundings is known as its corrosion potential (Ecorr), whereas the quantity of electron movement that is connected to the rate of corrosion in steel is known as its corrosion current (Icorr)[32]. Table 3 shows that sample 1 has an Icoor of 7.216 x 10-6 A/cm2 and a corrosion rate of 88.77 x 10-3 mmpy. The Ecorr of sample 1 is -647.1 mV. Ecorr was -615.7 mV in sample 2, Icoor was 3.571 x 10-6 A/cm2 and the corrosion rate was 41.46 x 10-3 mmpy. In sample 3, Ecorr was -1.023 mV with Icoor being 68.10 x 10-6 A/cm2 and the corrosion rate being 790.5 x 10-3 mmpy. With a hot rolling temperature of 1050°C, sample 3 readily reacts electrochemically with its surroundings and has a higher electron mobility, which leads to a rapid corrosion rate, according to the results [33].

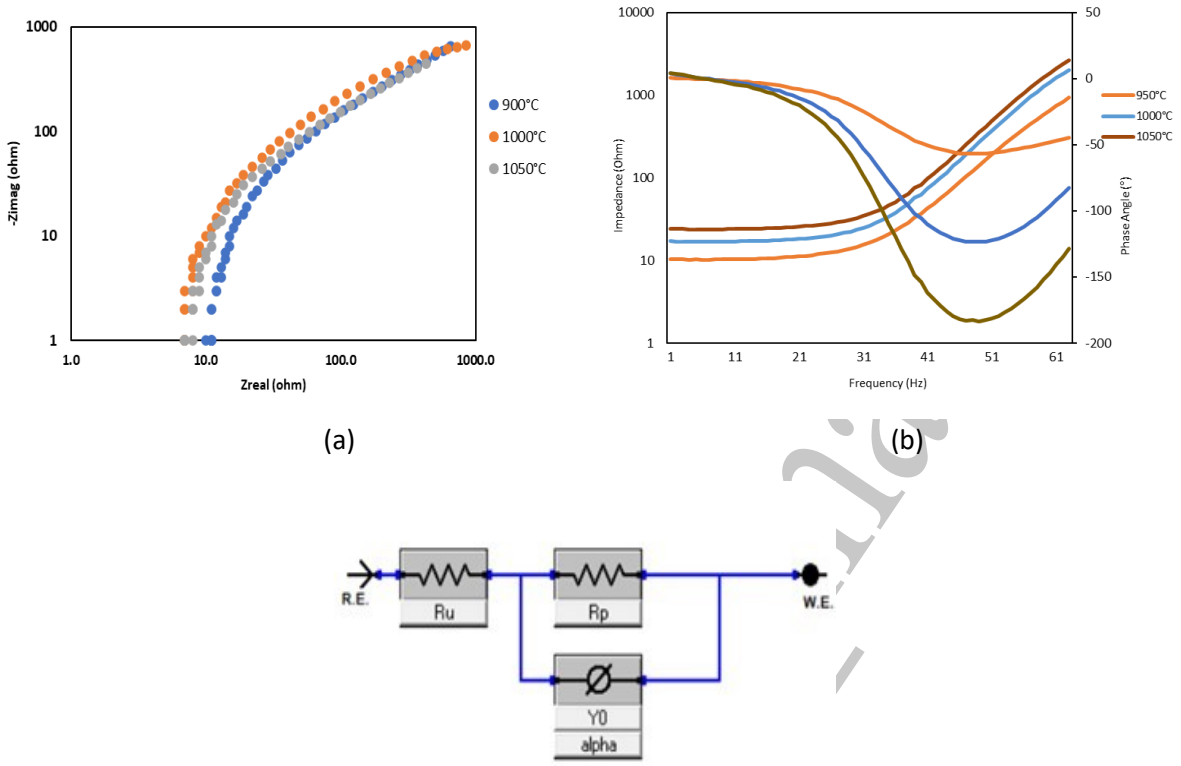

Figure 6. Eletrochemical Impedans Spectra of multilayer SDSS dan Baja karbon with variation temperature hot rolling (a) Nyquist plot (b) Bode plot (c) equivalent circuit model for EIS data fitting at open circuit potential in 5% NaCl.

Figure 6. shows the Electrochemical Impedance Spectra (EIS) of mild steel and multilayer SDSS after hot rolling. It also shows the equivalent circuit model for fitting EIS data at open circuit potential in 5% NaCl, as well as the Nyquist and Bode-modulus-phase plots.

The nyquist plot of EIS shows that the semicircular curve occurs in the high to low-frequency range in all types of steel. This indicates that all types of steel have two resistances, namely solution resistance (Ru) and charge transfer resistance (Rp). The circuit used for modeling the Nyquist plot of EIS is a simple Randless circuit model [34]. The equivalent circuit used for modeling the EIS results is shown in Figure 6 (c). The equivalent circuit used is the Constant Phase Element (CPE) equivalent circuit consisting of Ru, Rp, Yo, and alpha elements.

Table 3. Result of EIS fit for SDSS cladd mild steel in the 5% NaCl solution

Sample	Ru (Ω/cm^2)	Rp (Ω/cm^2)	Yo ($\mu S\ cm^{-2}\ s^a$)	Alpha
1	10.32	2.384e3	695.1e-6	696.8e-3
2	6.655	1.873e3	520.6e-6	800.5e-3
3	7.103	1.437e3	1.029e-3	738.1e-3

Based on Figure 4(a), the Nyquist curve with hot rolling temperature variations of 900°C, 1000°C, and 1050°C shows that diffusion happens at very low frequencies, meaning that the oxide layer formed is thin and discontinuous, allowing corrosion species to diffuse to the metal surface [35]. The rate of corrosion increases with increasing hot rolling temperature (table 3). When hot rolling at 1050°C, there is a fall in corrosion resistance and a smaller curve diameter on the Nyquist curve than when rolling at 900°C and 1000°C, which is followed by a drop in the Rp value (table 4). This suggests that the polarization resistance value will drop with increasing hot rolling temperature, increasing the rate of corrosion. The oxide layer that forms and has protective qualities is represented by the nyquist curve's high diameter. On the other hand, the nyquist curve's decreasing diameter suggests that the oxide layer that has developed is not continuous and that there are gaps or pores that allow diffusion to occur, which raises the rate of corrosion once more [36] The magnitude of impedance with phase shift is produced by the bode plot in Figure 5(b). The impedance increases at low frequencies as the hot rolling temperature rises (at low frequencies, it approaches ohmic resistance, which is the charge transfer resistance)[20]. A more unstable layer forms at greater hot rolling temperatures.

4. Summary

The study's findings indicate that the cladding process of mild steel and SDSS with hot rolling at temperatures of 900°C, 1000°C, and 1050°C results in a microstructure that varies between the mild steel and SDSS material sides and causes carburization and decarburization by diffusion. A temperature of 900°C results in a crystal structure that is FCC, at 1000°C it is BCC, and at 1050°C it is FCC. Ferrous exhibits anisotropic characteristics, meaning that its crystal structure varies with temperature. When hot rolling temperature reaches 1050°C, corrosion resistance starts to decline as the temperature rises, as seen by the rising rate of corrosion.

Acknowledgment

This work was supported by the Grant of Research Organization for Nanotechnology and Materials, National Research and Innovation Agency (BRIN) of the Republic of Indonesia.

Declarations Conflict of interest.

The authors declare that they have no known conflicts of interest

Author contributions

Lusiana: conceptualization, experimental work, investigation, resources, writing - original draft, writing - review and editing, and visualisation. Moch.Syaiful Anwar: supervision, visualization and validation. Permana Andi Paristiawan, Mustasyar Perkasa: technical support and process hot rolling. Adi Noer Syahid: technical support and help with SEM characterisation. Rahma Nisa Hakim: technical support and help with Microstructure characterisation. Yulinda Lestari: technical support and help with Elektrochemical characterisation. Kusdi Prijono: technical support and help with XRD characterisation.

Data Availability Statement

Data will be made available on request.

References:

[1] D. H. Abdeen, M. El Hachach, M. Koc, and M. A. Atieh, A review on the corrosion behaviour of nanocoatings on metallic substrates, Materials, 12 (2019) 1-42. https://doi:10.3390/ma12020210.

[2] Ying Han, Zheng-Hong Liu, Chun-Bo Wu, Yu Zhao, Guo-Qing Zu, Wei-Wei Zhu, Xu Ran, A short review on the role of alloying elements in duplex stainless steels, Tungsten, 5 (2023) 419–439. https://doi.org/10.1007/s42864-022-00168-z

[3] A. A. Mudha, H. D. Shashikala, and H. S. Nagaraja, Corrosion protection of low-cost carbon steel with SS-309Mo and Inconel-625 bimetallic weld overlay, Material Research Express, 6 (2019) 1-17. https://doi.org/doi: 10.1088/2053-1591/aafba6.

[4] A. Amudha, H. S. Nagaraja, and H. D. Shashikala, Finite element analysis of thermal residual stresses in SS-309Mo and Inconel-625 multilayer weld deposition on low carbon steel, International Journal of Fatigue, 127 (2019) 338–344. https://doi:10.1016/j.ijfatigue.2019.06.014.

[5] R. Francis and G. Byrne, Duplex stainless steels—alloys for the 21st century, Metals, 11 (2021) 1-23. https://doi.org/10.3390/met11050836

[6] B. Heider, M. Oechsner, U. Reisgen, J. Ellermeier, T. Engler, G. Andersohn, R. Sharma, E. Gonzalez Olivares, E. Zokoll, Corrosion Resistance and Microstructure of Welded Duplex Stainless Steel Surface Layers on Gray Cast Iron, Journal of Thermal Spray Technology, 29 (2020) 825–842. https://doi: 10.1007/s11666-020-01003-y.

[7] E. Atindra Joshi, S. Parkash, and E. Manoj Kumar, Study of Mechanical Properties, Microstructure and Corrosion Behavior of Super Duplex-2594 Weld Overlay on Carbon Steel Substrate by Smaw, Journal of Engineering Research and Application, 8 (2018) 65–70. https://doi: 10.9790/9622-0807016570.

[8] Liwei Wanga, Yi Ding, Qiankun Lub, Zhao Guo, Yuxi Liua, Zhongyu Cui, Microstructure and corrosion behavior of welded joint between 2507 super duplex stainless steel and E690 low alloy steel, Corrosion Communications, 11 (2023) 1-11. https://doi.org/10.1016/j.corcom.2022.08.005

[9] S. Yang, K. Cooke, H. Sun, X. Li, K. Lin, and H. Dong, Development of advanced duplex surface systems by combining CrAlN multilayer coatings with plasma nitrided steel substrates, Surface and Coatings Technology, 236 (2013) 2–7. https://doi:10.1016/j.surfcoat.2013.07.017.

[10] C. P. Paul, H. Alemohammad, E. Toyserkani, A. Khajepour, and S. Corbin, Cladding of WC-12 Co on low carbon steel using a pulsed Nd:YAG laser, Materials Science and Engineering, 464 (2007) 170–176. https://doi: 10.1016/j.msea.2007.01.132.

[11] K. T. Laitinen, H. Korhonen, J. T. T. Leskinen, A. Koistinen, and R. Lappalainen, Improved multilayer coatings by combined use of electrochemical and ultra-short pulsed laser deposition techniques, Surface and Coatings Technology, 300 (2016) 58–66. https://doi: 10.1016/j.surfcoat.2016.05.031.

[12] P. Murkute, S. Pasebani, and O. Burkan Isgor, Metallurgical and Electrochemical Properties of Super Duplex Stainless Steel Clads on Low Carbon Steel Substrate produced with Laser Powder Bed Fusion, Scientific Reports, 10 (2020) 1-19. https://doi:10.1038/s41598-020-67249-2.

[13] J. Liu, H. Liu, X. Tian, H. Yang, and J. Hao, Microstructural evolution and corrosion properties of Ni-based alloy coatings fabricated by multi-layer laser cladding on cast iron, Journal of Alloys and Compounds, 822 (2020) 1-11, https://doi:10.1016/j.jallcom.2020.153708.

[14] A M Bogatu, C Rontescu, R C Diacu, D-T Cicic, Research regarding strip cladding of heat-resistant SA 387 Gr.11Cl.2 steel type, Materials Science and Engineering, 1182 (2021) 1-6. https://doi:10.1088/1757-899X/1182/1/012008

[15] T. Gao, J. Wang, Q. Sun, and P. Han, Corrosion behavior difference in initial period for hot-rolled and cold-rolled 2205 duplex stainless steels, Metals, 8 (2018) 2-13, https://doi: 10.3390/met8060407.

[16] A. A. Mudha, H. D. Shashikala, and H. S. Nagaraja, Corrosion protection of low-cost carbon steel with SS-309Mo and Inconel-625 bimetallic weld overlay, Material Research Express, 6 (2019) 1-17, https://doi: 10.1088/2053-1591/aafba6.

[17] M. H. E. Seshweni, A. Moloto, S. Aribo, S. R. Oke, O. O. Ige, and P. A. Olubambi, Influence of cold and hot rolling on the corrosion behaviour of duplex stainless steels in mine water environment, Materials Today, Proceedings (2019) 1-4. https://doi:10.1016/j.matpr.2019.12.323.

[18] M. Herrmann, C. Schenck, H. Leopold, and B. Kuhfuss, Material improvement of mild steel S355J2C by hot rotary swaging, Procedia Manufacturing, 47 (2020) 282–287. https://doi: 10.1016/j.promfg.2020.04.224.

[19] G. Yuan, P. Han, X. Zhu, Z. Jiang, and X. Wang, Fabrication of a Composite Material of High-Chromium Cast Iron Dispersed in Low-Carbon Steel by Hot-Rolling Process, Steel Research International, 92 (2021) 1-10, https://doi: 10.1002/srin.202100001.

[20] B. Heider, M. Oechsner, U. Reisgen, J. Ellermeier, T. Engler, Corrosion Resistance and Microstructure of Welded Duplex Stainless Steel Surface Layers on Gray Cast Iron, Journal of Thermal Spray Technology, 29 (2020) 825–842. https://doi: 10.1007/s11666-020-01003-y.

[21] Y. Han, J. Shi, L. Xu, W. Q. Cao, and H. Dong, Effect of hot rolling temperature on grain size and precipitation hardening in a Ti-microalloyed low-carbon martensitic steel, Materials Science and Engineering: A, 553 (2012) 192–199. https://doi: 10.1016/j.msea.2012.06.015.

[22] Designation: A213/A213M − 13 Standard Specification for Seamless Ferritic and Austenitic Alloy-Steel Boiler, Superheater, and Heat-Exchanger Tubes, ASTM International, 0101 (2018) 1-14.

[23] E. M. Cojocaru, D. Raducanu, A. Nocivin, and V. D. Cojocaru, Influence of ageing treatment temperature and duration on σ-phase precipitation and mechanical properties

of UNS S32750 SDSS alloy, Journal of Advanced Research, 30 (2021) 53–61. https://doi: 10.1016/j.jare.2020.11.005.

[24] K. O. Cooke and A. M. Atieh, Current trends in dissimilar diffusion bonding of titanium alloys to stainless steels, aluminium and magnesium, Journal of Manufacturing and Materials Processing, 4 (2020) 1-22. https://doi: 10.3390/jmmp4020039.

[25] Y. Yang, Z. Jiang, X. Liu, J. Sun, and W. Wang, Enhanced interfacial strength and ductility of stainless steel/carbon steel laminated composite by heterogenous lamella structure, Journal of Materials Research and Technology, 18 (2022) 4846–4858. https://doi: 10.1016/j.jmrt.2022.04.057.

[26] Y. Yang, Z. Jiang, Y. Chen, X. Liu, J. Sun, and W. Wang, Interfacial microstructure and strengthening mechanism of stainless steel/carbon steel laminated composite fabricated by liquid-solid bonding and hot rolling, Journal of Materials Research and Technology, 191 (2022) 4846-4858. https://doi: 10.1016/j.matchar.2022.112122.

[27] F. Xiao, D. Wang, Z. Gao, and L. Zhou, Effect of heating process on microstructure and properties of 2205/Q235B composite interface, Metals, 9 (2019) 2-17. https://doi:10.3390/met9101027.

[28] K. T. Moore, D. E. Laughlin, P. Söderlind, and A. J. Schwartz, Incorporating anisotropic electronic structure in crystallographic determination of complex metals: Iron and plutonium, Philosophical Magazine, 87 (2007) 2571–2588. https://doi:10.1080/14786430701241697.

[29] U. Dey, N. Mitra, and A. Taraphder, High temperature–high pressure phase transformation of Cu, Computational Materials Science, 170 (2019) 1-7. https://doi:10.1016/j.commatsci.2019.109154.

[30] Y. Z. Yang, Y. M. Jiang, and J. Li, In situ investigation of crevice corrosion on UNS S32101 duplex stainless steel in sodium chloride solution, Corrosion Science, 76 (2013) 163–169, https://doi: 10.1016/j.corsci.2013.06.039.

[31] C. Torres, R. Johnsen, and M. Iannuzzi, Crevice corrosion of solution annealed 25Cr duplex stainless steels: Effect of W on critical temperatures, Corrosion Science, 178 (2021) 1-14. https://doi: 10.1016/j.corsci.2020.109053.

[32] M. Abdelbar and A. M. El-Shamy, Understanding soil factors in corrosion and conservation of buried bronze statuettes: insights for preservation strategies, Scientific Reports, 14 (2024) 1-28. https://doi: 10.1038/s41598-024-69490-5.

[33] J. Akpoborie, O. S. I. Fayomi, O. Agboola, O. D. Samuel, B. U. Oreko, and A. A. Ayoola, Electrochemical Corrosion Phenomenon and Prospect of Materials Selection in Curtailing the Challenges, Materials Science and Engineering, 1107 (2021) 1-10. https://doi: 10.1088/1757-899x/1107/1/012072.

[34] M. S. Anwar, T. B. Romijarso, and E. Mabruri, Pitting resistance of the modified 13Cr martensitic stainless steel in chloride solution, International Journal of Electrochemical Science, 13 (2018) 1515–1526. https://doi: 10.20964/2018.02.13.

[35] V. Encinas-Sánchez, M. T. de Miguel, M. I. Lasanta, G. García-Martín, and F. J. Pérez, Electrochemical impedance spectroscopy (EIS): An efficient technique for monitoring corrosion processes in molten salt environments in CSP applications, Solar Energy Materials and Solar Cells, 191 (2019) 157–163. https://doi:10.1016/j.solmat.2018.11.007.

[36] M. Swayne, G. Perumal, D. B. Padmanaban, D. Mariotti, and D. Brabazon, Exploring the impact of laser surface oxidation parameters on surface chemistry and corrosion behaviour of AISI 316L stainless steel, Applied Surface Science Advances, 22 (2024) 1-13. https://doi: 10.1016/j.apsadv.2024.100622.